REPORT DOCUMENTATION PAGE

Form Approved
OMB No. 0704-0188

1. REPORT DATE *(DD-MM-YYYY)*	2. REPORT TYPE	3. DATES COVERED *(From - To)*
	Technical Paper	

4. TITLE AND SUBTITLE

5a. CONTRACT NUMBER

5b. GRANT NUMBER

5c. PROGRAM ELEMENT NUMBER
62500F

6. AUTHOR(S)

5d. PROJECT NUMBER
2308

5e. TASK NUMBER
M4S7

5f. WORK UNIT NUMBER
345382

7. PERFORMING ORGANIZATION NAME(S) AND ADDRESS(ES)

8. PERFORMING ORGANIZATION REPORT

9. SPONSORING / MONITORING AGENCY NAME(S) AND ADDRESS(ES)

Air Force Research Laboratory (AFMC)
AFRL/PRS
5 Pollux Drive.
Edwards AFB CA 93524-7048

10. SPONSOR/MONITOR'S ACRONYM(S)
XC

11. SPONSOR/MONITOR'S NUMBER(S)

12. DISTRIBUTION / AVAILABILITY STATEMENT

Approved for public release; distribution unlimited.

13. SUPPLEMENTARY NOTES

See attached 8 papers, all with the information on this page.

14. ABSTRACT

15. SUBJECT TERMS

16. SECURITY CLASSIFICATION OF:			17. LIMITATION OF ABSTRACT	18. NUMBER OF PAGES	19a. NAME OF RESPONSIBLE PERSON
a. REPORT	b. ABSTRACT	c. THIS PAGE			Kenette Gfeller
Unclassified	Unclassified	Unclassified	A		19b. TELEPHONE NUMBER *(include area code)* (661) 275-5016

ICE TECHNOLOGY & APPLICATIONS FORUM (STAIF-97), Albuquerque NM
Jan 26-30, 1997

PROPELLANT INEFFICIENCY DUE TO PARTICULATES IN A PULSED PLASMA THRUSTER

Gregory G. Spanjers
Hughes STX Corporation
Edwards AFB, CA 93524
(805) 275-5907

Jason S. Lotspeich, Keith A. McFall, Ronald A. Spores
Propulsion Directorate, OL-AC Phillips Laboratory
Edwards AFB CA 93524
(805) 275-5528

Abstract

Propellant inefficiency resulting from the ejection of propellant material in particulate form is characterized in a Pulsed Plasma Thruster (PPT). Exhaust deposits are collected and analyzed using a combination of Scanning Electron Microscope (SEM), Energy Dispersive X-ray Analysis (EDAX), and microscopic imaging. Teflon particulates are observed with sizes ranging from over 100 μm down to less than 1 μm. Estimates of the mass entrained in this form show that the particulates may account for up to 30% of the total propellant mass used, indicating that methods of ameliorating this loss mechanism would result in significant improvements in the PPT thrust efficiency.

INTRODUCTION

The Pulsed Plasma Thruster (PPT)(Guman et al. 1970) is an attractive propulsion option for small power-limited satellites. The PPT, shown schematically in Fig. 1, operates at low power levels (<100W) by charging an energy-storage capacitor on a long time scale (1 sec), and then discharging on a short time scale (10 μs) at high instantaneous power. High reliability is achieved through the use of a solid propellant (typically Teflon) which eliminates the complexity and dry mass associated with gaseous propellants. The only moving part on the PPT is a spring which passively feeds the propellant into the discharge chamber. The solid propellant is converted to vapor and partially ionized by a surface discharge across the propellant face. Acceleration is accomplished by a combination of thermal and electromagnetic forces to create usable thrust. The inherent engineering advantages of the PPT design have enabled the thruster to complete several space missions over the past 30 years with no failures. Present PPT missions (Tilley et al. 1996) include using the thruster for orbit-raising the Phillips Laboratory MightySat spacecraft (1999 launch). Unfortunately the excellent engineering characteristics of the PPT are coupled with poor performance characteristics. Flight-qualified designs (Vondra 1976) have achieved thrust efficiencies ($h = T^2/2mE$) below 8%. The low thrust efficiency is attributable to both a low energy efficiency and a low propellant efficiency. (Spanjers et al. 1996, Solbes et al. 1973) Previous measurements have shown that neutral gas vaporizing from the propellant face long after the current discharge is a significant factor in the low propellant efficiency. (Spanjers 1996, Solbes et al. 1973) Theoretical modeling has also identified propellant inefficiency as a serious impediment to improving PPT performance. (Mikellides et al. 1996)

In the present work a second mechanism, particulate emission, is identified as a significant contributor to the low propellant efficiency. Broadband emission indicative of particulates is observed emitting from the PPT long after the current pulse. Scanning Electron Microscopy (SEM) of exhaust deposits shows particulates in agreement with the emission measurements. Energy Dispersive X-ray Microanalysis (EDAX) identifies the particulates as Teflon. The propellant mass expended in particulate form is estimated to be 30% of the total mass ablated during the PPT discharge. PPT design improvements directed at eliminating particulate formation would result in increased propellant efficiency and a concomitant increased thrust efficiency.

EXPERIMENTAL APPARATUS

The experiments are performed at the Edwards AFB location of the Air Force Phillips Laboratory in Chamber 5 of the Electric Propulsion Laboratory. The experiments are performed on the exhaust from XPPT-1 (Experimental Pulsed Plasma Thruster #1) shown in Fig. 2. (Spanjers 1996)

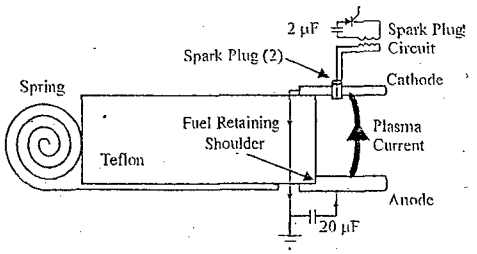

FIGURE 1. Schematic of a Pulsed Plasma Thruster.

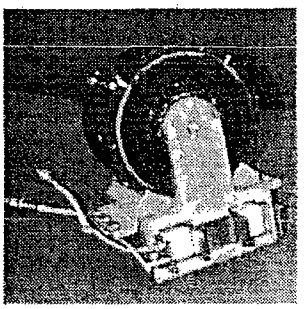

FIGURE 2. XPPT-1 Pulsed Plasma Thruster.

Broadband light emission is digitally recorded using a high-speed framing camera. The camera has only single-frame capability so images at different times and shutter speeds are recorded on different PPT discharges. Camera sensitivity increases exponentially with gain. Exhaust samples are collected on disks of 6061-T6 aluminum, 12.7 mm. dia. and 3.2 mm thick. The aluminum sample substrate is chosen since its composition is well known, and its conductivity helps minimize sample charging during SEM analysis.

Energy dispersive X-ray microanalysis (EDAX) is used to determine the composition and relative concentration of elements on the sample disks. The electron beam, used for imaging the deposits in the SEM mode, is used at higher energy to excite X-ray transitions within the sample elements. To insure excitation of at least one X-ray series (K, L or M) for each of the elements under investigation, an accelerating voltage of 15-20 keV is required. However, these higher energy electrons have decreased resolution for the lighter elements (fluorine and carbon) expected on the sample surface. Thus, lower accelerating voltages (under 10 keV) are optimal for examining lighter elements, and higher accelerating voltages are optimal for examining heavier elements, with an expected loss in resolution for X-rays from lighter elements.

The principal materials expected in the EDAX analysis are from the Teflon propellant (33% C, 66% F), 304 Stainless Steel electrodes (.08% C, 69% Fe, 19% Cr, 9% Ni, <2% Mn, <1% Si), and the 6061-T6 aluminum sample disk (97.9% Al, 1% Mg, 0.6% Si, 0.25% Cr, 0.25% Cu). Particles on the sample surface with strong carbon and fluorine X-ray emission are presumed to have been deposited as Teflon (C_2F_4). If the Teflon had disassociated prior to deposition, it is assumed that the gaseous fluorine would have pumped out of the system leaving only a carbon deposit.

EXPERIMENTAL RESULTS

Experiments are performed using XPPT-1 configured with a 20 μF capacitor and charged to 1414 V for a discharge energy of 20 J. The discharge has a peak current of 15 kA and decays in 20 μs with approximately 4 current oscillations. The thruster is operated at 1/8 Hz corresponding to an average power level of 2.5 W. The aluminum sample disks are spread in arrays orientated parallel and perpendicular to the PPT electrodes in order to quantify the spatial distribution of exhaust deposits. Parallel to the electrodes, samples are positioned every 30 degrees. Perpendicular, samples are positioned every 45 degrees. All sample disks are located 6 cm from the center of the propellant face. Deposits on the sample disks are accumulated over 1000 PPT discharges. The fuel bar had been previously discharged approximately 10,000 times prior to the experimental runs, so that a slightly concave shape had been eroded into the propellant face. A propellant mass ablation rate of 15 μg/discharge was calculated from measurements of the propellant mass prior to and after the 1000 discharge test.

Broadband emission from the PPT exhaust is shown in Fig. 3. Figure 3a is recorded during the discharge with a 10 μs shutter and gain of 300. The emission is suggestive of a standing arc near the propellant face with streams of plasma accelerated in the thrust direction. The exhaust appears distributed and devoid of particulates. Reduction of the shutter time to 50 ns also shows no evidence of particulates, although the discharge becomes substantially more filamentary. Figure 3b is recorded 100 μs after the discharge with a 10 μs shutter and gain of 800 V. Numerous localized emission sites are apparent. The absence of discharge energy at this time, coupled with previous measurements of a high-density neutral vapor,[6] indicates that the propellant face is continuing to vaporize. Figure 3c is recorded at the same experimental time as Fig. 3b but with a longer 100 μs shutter and gain of 450 V. The

emission now appears as streaks showing the motion of the emission sites. For the characteristic streak length of 2 cm, a velocity of approximately 200 m/s is inferred. The duration of the streak emission (~100 μs) implies a heat capacity incompatible with a single molecule or plasma motion, requiring the higher mass of particulates.

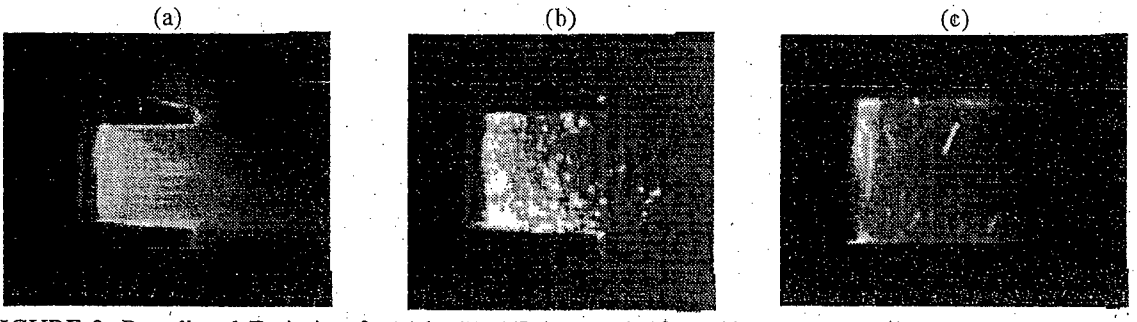

FIGURE 3. Broadband Emission from the PPT Exhaust, a) 10 μs Shutter During the Discharge, b) 10 μs Shutter Initiated 100 μs After the Discharge, c) 100 μs Initiated Shutter 100 μs After the Discharge.

To support the hypothesis of the presence of particulates in the PPT exhaust suggested by the broadband emission, the sample disks were placed in the exhaust and subjected to surface analysis. SEM imaging of the exhaust deposits shows material concentrations, attributable to particulates striking the sample, superimposed on a background film. Figure 4 shows an SEM image of a particulate deposit at 1100X magnification. The deposit is approximately 690 mm^2 in area and is surrounded by a circular structure suggestive of the crater formation associated with particle impact. SEM imaging at reduced magnification (369X), Fig. 5, shows four particle deposits of size similar to that in Fig. 5. The particles appear bright in the SEM photograph which occurs when the electron beam electrically charges the deposit. This indicates that the deposited material is an insulator, unable to conduct excess charge to the substrate, suggesting that the deposits are composed of Teflon. A multitude of smaller sized deposits are also apparent in Fig. 5.

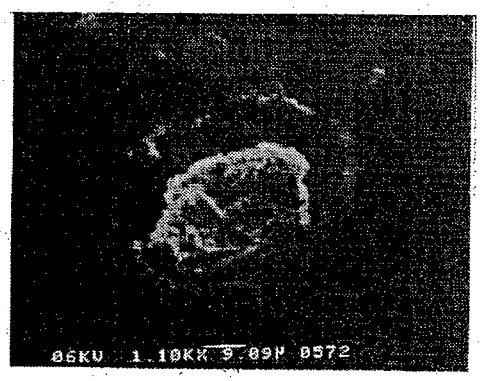

FIGURE 4. SEM Image Magnified 1100X.

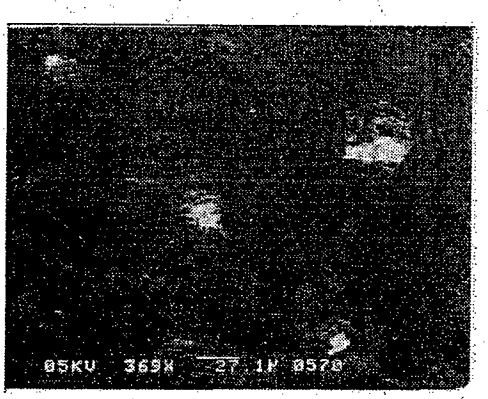

FIGURE 5. SEM Image at 369X Magnification.

The EDAX Spectra from the particle in Fig. 4 and the background film that coats the substrate are tabulated in Table 1. Also listed are the calibration spectra for the propellant (Teflon) and electrode (304 Stainless Steel) materials. Line intensities are normalized to the signal at 700 eV, which is identified as either F or Fe within the resolution of the EDAX, and the intensities are tabulated for both low and high EDAX electron accelerating potential. The difficulty in separating the critical elements is apparent in the low energy case where the spectral peaks for Teflon and steel both consist primarily of lines at 200 eV and 700 eV. At high energy both materials again share the peaks at 200 eV and 700 eV however the steel also shows large intensity at higher energy transitions corresponding to Cr, Fe and Ni. The Teflon also shows small signals at the Ni transitions attributable to emission from either the EDAX chamber or the sample mount. The small steel transition lines in the background and particle EDAX spectra shows that these components are not principally comprised of steel. The small steel transition signal that is observed implies that some electrode material is deposited, possibly at higher concentration in the background than in the particle. At both energy levels the spectra for the particle and for the background film are approximately equal. A possible cause is that the background film contains of a large population of particles deposited at

characteristic sizes less than that detected with the SEM. This would preclude a true EDAX analysis of the background film since a multitude of particulates would always be present, skewing the results towards the spectra of a particulate. Comparison of the Teflon and particulate spectra for the low energy case shows that the particulate is carbon-rich. This may result from co-sampling background film that has deposited on or below the particle. A total of 8 particle deposits were identified through SEM and characterized through EDAX. Each of these was concluded to be comprised of Teflon as opposed to 304 Stainless Steel, although all were found to be carbon-rich similar to the EDAX spectra of Table 1.

TABLE 1: Normalized Spectral Line Intensities for the Background Film, a Particulate Deposit, and Calibration Spectra of Teflon and 304 Stainless Steel. Intensities are Shown for Both Low and High Energy EDAX Electrons.

		F or Fe 700 eV	C 200 eV	Cr 450 eV	Cr 5900 eV	Fe 6500 eV	Ni 7100 eV	Ni 7500 eV
Low Energy	Teflon	1	0.29	0	0	0	0	0
(6 -7 keV)	304 SS	1	offscale	0.047	0	0	0	0
	Background	1	1.3	0	0	0	0	0
	Particulate	1	1.4	0	0	0	0	0
High Energy	Teflon	1	0.31	0	0	0	0.019	0.030
(15 - 20 keV)	304 SS	1	offscale	2.4	.38	5.8	0.75	0.46
	Background	1	2.9	.075	0	0.15	0.025	0.075
	Particulate	1	3.3	.037	0	0.11	0.0074	0.074

Images at several magnifications, Fig. 6, illustrate the particle size distribution. A full range of particle sizes are observed from a multitude of particles near 1μm in the 100X image to two large particles 200 μm long observed in the 5X image. The large particle in the 5X image is part of a streak of several particles that appear to have been deposited as a group. Presumably a relatively large mass struck the sample disk at a slight angle to create several deposits aligned in a single streak. Two such groupings were found on the sample disk.

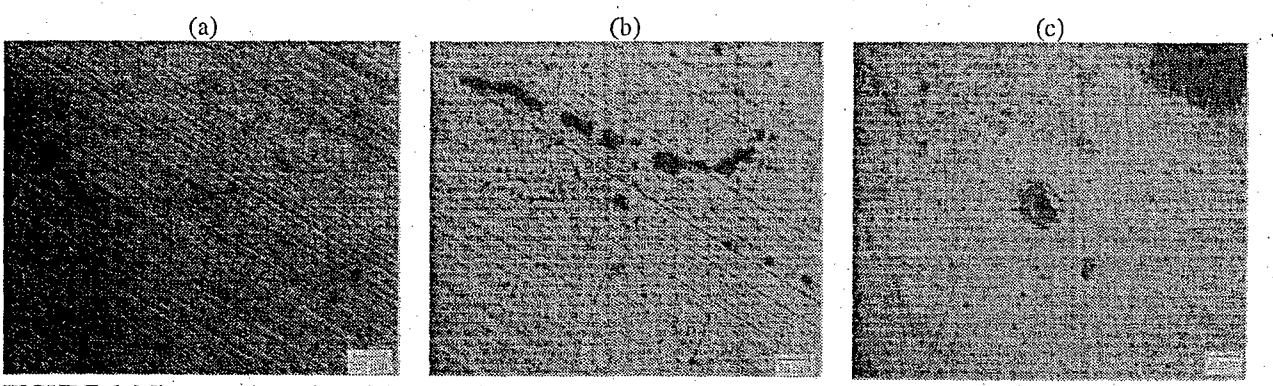

FIGURE 6. Microscope Images of the Sample Deposits, a) 5X, b) 20X, and c)100X Magnification.

Measurements of the spatial distribution of the particulate mass deposits shows a cosine dependence, although more peaked for the distribution perpendicular to the electrodes. The mass is calculated by counting the number of particles on each disk with diameters in excess of 50 μm, using 10X microscope images. The normalized mass is assumed to be proportional to the number of these large particles. This analysis assumes either that the bulk of the sample mass is contained in the large particles or that the spatial distribution of other particle sizes is similar to that of the large particles. A more accurate calculation of the total particulate mass deposited on the sample at 0° is accomplished in the following section by counting particles down to 15 μm in diameter.

DISCUSSION

A critical question is whether exhaust in the particulate form accounts for a significant fraction of the propellant usage in the PPT. The total particulate mass can be estimated from Fig. 6a which shows a 2.3 mm x 3.0 mm area of the sample disk magnified at 5X. The particle sizes in Fig. 6a are tabulated by their general size group in Table 2. In

the mass calculations for Table 2, the height of each deposit is estimated to be equal to the radius and the volume is calculated as a half-sphere: $V=2pr^2h/3$. Density is assumed to be that of Teflon. This analysis estimates a total of 2.7 μg to be in particulate form in Fig. 6a. This mass is scaled by the relative areas of the image to the area of the sample disk to estimate 51 μg of particle deposits on the sample disk, equivalent to 0.37% of the total propellant mass ablated during the 1000 discharge experiment. This estimate ignores particles below 15 μm in diameter which could have a significant impact on the total mass. Also ignored are the two large streak formations observed on the sample disk, which would add approximately 0.5 μg to the total sample disk mass. These are ignored since only two formations on the entire disk surface is an insufficient statistical sampling.

TABLE 2. Size Distribution and Estimated Mass for the Particle Deposits of Fig. 6a.

Diameter (μm)	Number	Total Mass (μg)
15 - 25	105	0.45
25 - 50	20	0.59
50 - 75	4	0.55
75 - 100	2	1.1
Total Particle Mass		2.7

The total particulate mass emitted by the PPT is estimated by integrating the measured spatial distribution over the solid angle in front of the thruster, normalized to the mass calculated to be deposited on the sample disk at 0°. This results in a total particle mass emitted by the PPT of 4.5 mg which is 30% of the total propellant usage in the experiment. The analysis shows the particulate mass to be a significant contributor to the propellant inefficiency in the PPT, possibly as important as the late time vaporization (Spanjers et al. 1996, Mikellides et al. 1996) Note that particles were only counted in sizes down to 15 μm diameter. Since the smaller particles have the potential to contribute significantly to the total particulate mass, and since the large streak deposits were not included in the estimate, it is possible that the propellant loss in the form of particulates may be the dominant source of propellant inefficiency in the PPT.

Understanding the mechanism behind the creation of the particulates is critical to eventually minimizing this loss mechanism in PPTs. Vaporization beneath the propellant face, due to radiation transmission a finite depth into the Teflon, would result in high gas pressures that would explosively eject the particulates. Emission streaks in Fig. 3 imply that a significant fraction of particles appear to originate from the electrodes. This may be a result of Teflon vapor from previous discharges condensing on the electrode surface. Localized heating from the plasma arc then vaporizes electrode material beneath the condensed Teflon causing particle ejection. Traces of steel in the background film deposits confirm that some electrode vaporization is occurring. The emission images imply that particulate ejection from the electrodes occurs well after the discharge with no detectable particulates during the PPT current. This may actually result from the relatively strong emission from the plasma arc overwhelming the weaker emission from the particulates. The image during the discharge, Fig. 3a, was obtained with a camera gain of 300, which would be insufficient to record the emission 100 μs after the discharge when particulates are apparent, Fig. 3b. It is also important to note that the streaks apparent in Fig. 3c may not be responsible for the Teflon deposits on the sample disks. The Teflon particles may be emitted at low temperature from the propellant face and never be observable with the camera due to a low light emission level.

The experimental design of XPPT-1 compared to the flight-qualified LES 8/9 PPT brings into question whether the particle emission is specific to only the thruster considered in the present work. Similar results have been reported (Myers et al. 1996) from contamination tests on the LES 8/9 PPT. In that work SEM analysis was used to observe a large number of 1 to 5 μm particles superimposed on a base film, in agreement with the present work. Presumably images at other magnifications would have also yielded results similar to those reported here. The contamination test work also reported a small number of metal particles that may have originated from the electrodes. No such metal particles were observed in the present work, however this is probably due to the relatively few number of particles that were examined using EDAX.

The present work is concerned solely with sources of propellant inefficiency in the PPT to better guide future thruster designs. No conclusions can be made as to the possible contamination effects of the particles on the spacecraft surfaces. The XPPT-1 is of inappropriate design for contamination studies since it lacks the housing

around the electrodes that a flight unit would certainly have. A dedicated contamination study for the PPT has been performed using a flight-qualified PPT (LES 8/9). (Myers et al. 1996) No measurable deposition was observed in the backflow region of the thruster, indicating that contamination is not a major concern for these devices.

SUMMARY AND CONCLUSIONS

Surface analysis on exhaust deposits from the PPT reveal a significant quantity of propellant material in particulate form. Estimates of the total mass exhausted in this form show that particulates may account for 30% of the total propellant usage indicating that this is a significant, and possibly dominant, source of propellant inefficiency in these devices. One source of the particulates is believed to be energy deposition below the Teflon surface. This energy vaporizes material behind the propellant face creating a high gas pressure that results in material ejection in the form of particles. A second potential source of ejected particles results from vaporized Teflon propellant condensing on the electrode. During subsequent PPT discharges electrode vaporization beneath the coating ejects the Teflon material as particulates. Research directed towards minimizing the particle ejection can have a significant impact on PPT thrust efficiency. Present research at Phillips Laboratory is exploring the use of propellants with reduced transmission in an effort to deposit the arc radiation energy in a minimally thin layer at the propellant face. Additional research is directed towards reducing the late-time propellant vaporization in order to decrease the amount of propellant condensed on the electrode surfaces.

Acknowledgment

Jason Lotspeich is a graduate student of Mechanical Engineering at Colorado State University, Fort Collins. He conducted this research at AF Phillips Laboratory supported through the Air Force Office of Scientific Research under the Graduate Summer Research Program. The authors acknowledge the assistance of Richard von Lutz and Paul Jones of the Phillips Laboratory, Propulsion Directorate, Propulsion Sciences Division in performing the SEM/EDAX analysis.

Reference

W. J. Guman and D. M. Nathanson, "Pulsed Plasma Microthruster for Synchronous Orbit Satellite," *J. Spacecraft and Rockets*, Vol. 7, No. 4, 1970, pp. 409-415.

P. G. Mikellides and P. J. Turchi, "Modeling of Late-Time Ablation in Teflon Pulsed Plasma Thrusters," 32nd AIAA/ASME/SAE/ASEE Joint Propulsion Conference, AIAA Paper 96-2733, Lake Buena Vista, FL, July 1-3, 1996.

R. M. Myers, L. A. Arrington, E. J. Pencil, J. Carter, J. Heminger, and N. Gatsonis, "Pulsed Plasma Thruster Contamination," 32nd AIAA/ASME/SAE/ASEE Joint Propulsion Conference, AIAA Paper 96-2729, Lake Buena Vista, FL, July 1-3, 1996.

D. L. Tilley, J. A. Pobst, D. R. Bromaghim, R. M. Myers, R. J. Cassady, W. A. Hoskins, N. J. Meckel, J. J. Blandino, D. E. Brinza, M. D. Henry, "Advanced Pulsed Plasma Thruster Demonstration on MightySat Flight II.1," 2nd Utah State Univ./AIAA Conf. On Small Satellites, Logan, UT, Sept. 1996.

A. Solbes and R. J. Vondra, "Performance Study of a Solid Fuel Pulsed Electric Microthruster," *J. Spacecraft*, Vol. 10, No. 6, 1973, pp. 406-410.

G. G. Spanjers, K. A. McFall, F. S. Gulczinski III and R. A. Spores, "Investigation of Propellant Inefficiencies in a Pulsed Plasma Thruster," 32nd AIAA/ASME/SAE/ASEE Joint Propulsion Conference AIAA Paper 96-2723, Lake Buena Vista, FL, July 1-3, 1996.

R. J. Vondra, "The MIT Lincoln Laboratory Pulsed Plasma Thruster," AIAA International Electric Propulsion Conference, AIAA Paper 76-998, Key Biscayne, FL, Nov. 14-17, 1976.